

Undulating topography on the Antarctic ice sheet revealed by NOAA AVHRR images

KATSUMOTO SEKO AND TERUO FURUKAWA
Water Reserach Institute, Nagoya University, Nagoya 464-01, Japan

FUMIHIKO NISHIO
Hokkaido University of Education, 1-15-55, Shiroyama, Kushiro 085, Japan

OKITSUGU WATANABE
National Institute of Polar Research, Kaga, Itabashi, Tokyo 173, Japan

ABSTRACT. Undulating topography on the East Antarctic ice sheet was clearly revealed by NOAA AVHRR. The following three patterns of undulating topography were detected by using high-pass filtered images from the visible to thermal infrared channels. In coastal regions (below 2000 m a.s.l.), undulation can be clearly detected by the fluctuation of reflectance in visible channel. It has wavy structure with spacing less than 10 km and alignment at a right angle to the ice-flow lines. In the katabatic zone (from 2000 m a.s.l. to 3000 m a.s.l.) well defined fluctuations of albedo spectrum can be seen with spacing from 10 km to 20 km, aligned at right angles to the ice-flow lines or prevailing katabatic wind direction. Ground-survey data show that the undulating topography is associated with large variations of net accumulation rate. On the inland plateau (above 3000 m a.s.l.), undulation can be clearly seen in the fluctuation of thermal infrared channel in winter. Ground-survey data show that the signal corresponds to the undulating topography. The alignment of the undulation is at a right angle to the ice-flow lines and the spacing is longer than 20 km. The characteristics of these undulations represent the ice-flow dynamics and accumulation anomaly.

INTRODUCTION

The surface of the Antarctic ice sheet is neither smooth nor uniform. It is dynamic as a result of ongoing climatological and glaciological processes. The detail structure of undulating topography on the surface contains information on ice-sheet dynamics.

Meso-scale (less than 100 km in horizontal scale) undulating topography has been studied by several methods. Although intensive field studies (Watanabe, 1978; Furukawa and others, 1992) can provide invaluable data, the area covered by a field scientist is relatively small and two-dimensional aerial distribution of undulations or surface features has been poorly known.

Remote sensing is a powerful tool for the investigation of ice-sheet surface (Seko and others, 1992, NIPR, 1992). The ice sheet, especially in the coastal region, was intensively investigated by using Landsat images (Orheim and Lucchitta, 1987, 1988; Swithinbank, 1988; Stephenson and Bindshadler, 1990). However, the aerial coverage of a Landsat image is too small to survey the vast area of the ice sheet at reasonable cost.

The advantage of NOAA AVHRR (Advanced Very High Resolution Radiometer) is its wide areal coverage. It is just beginning to be used for glaciological features

(Fujii and others, 1987; Bindshadler and Vornberger, 1990). We can view half of the East Antarctic ice sheet by using data obtained at Syowa Station, Antarctica. The main objective of this study is to describe the surface undulating topography detected from satellite images in the area and their causes of visualization, and discuss their origins.

DATA AND IMAGE PROCESSING

NOAA AVHRR data received at Syowa Station, Antarctica (NIPR, 1992) were used. Channel 1 (visible: 0.5–0.6 μm), Channel 2 (near infrared: 0.725–1.1 μm) Channel 4 (thermal infrared: 10.5–11.5 μm) and the ratio of Channel 2 to Channel 1 (hereafter, R2/1 will be used for this value) were used in this study.

The processed images have resolutions from 1.1 km to 4.4 km depending on its areal extent. The accuracy of position on the images is controlled within a few km by matching geodetic ground-control points such as outstanding rocks or bare ice fields. Corresponding ground-survey data were obtained by over-snow traverse observations (Nishio and others, 1988b; Ageta and others, 1987).

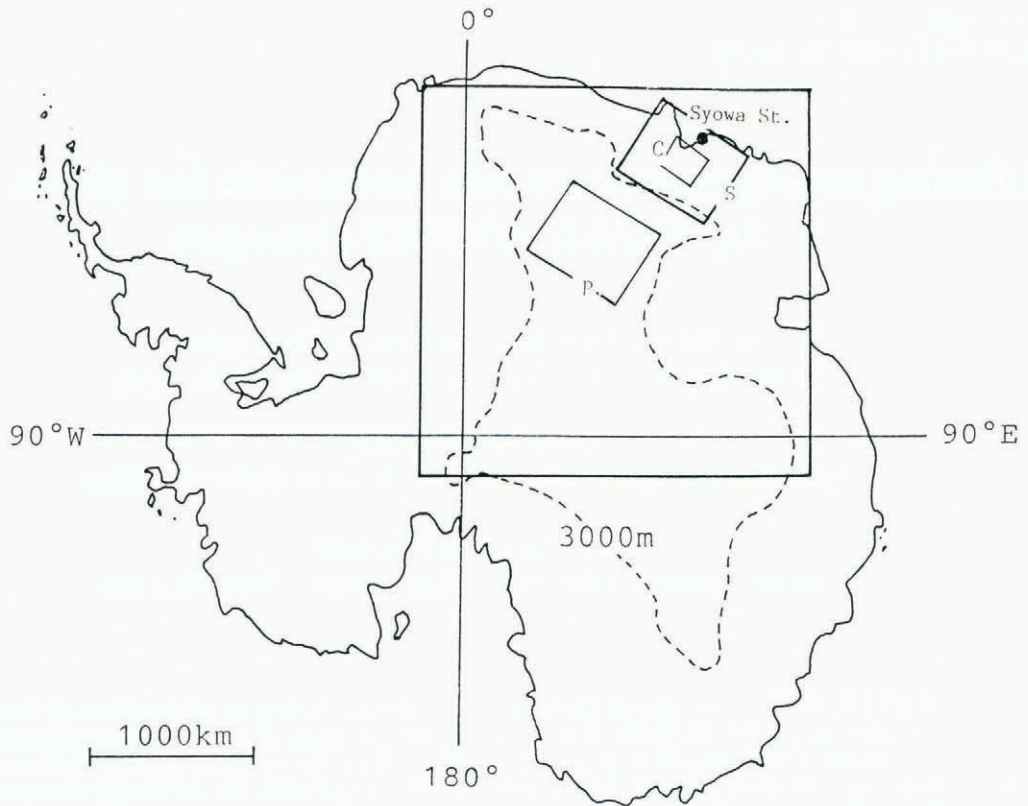
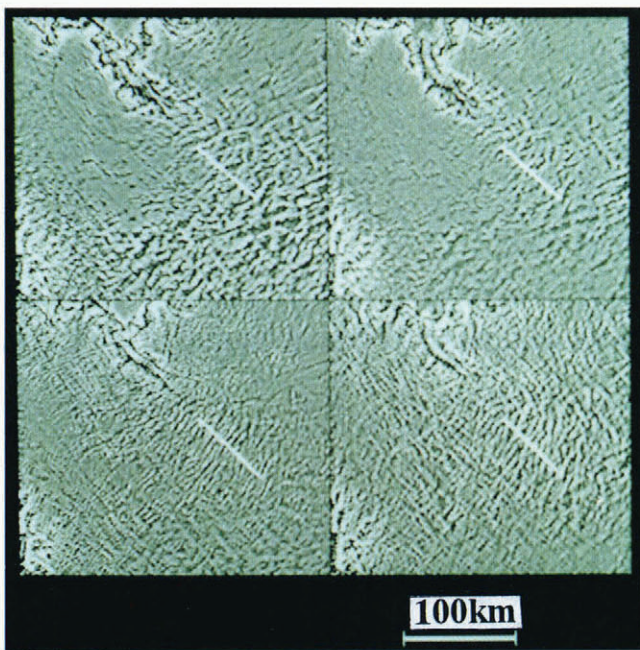


Fig. 1. Areas of NOAA AVHRR images. The 3000 m surface elevation contour is shown as a dashed line. C, S, P and M mean the areas of Figures 2a, 4a, 6a and 8, respectively.

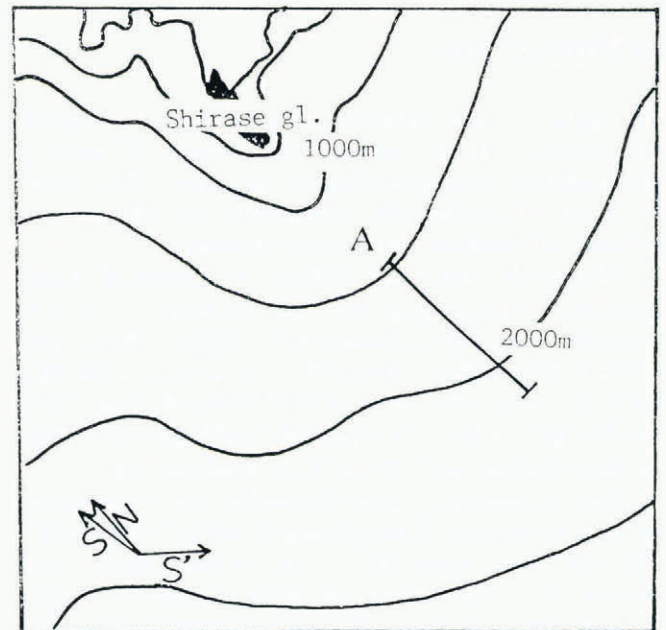
A spatial high-pass filter was applied for the enhancement of structures of less than 100 km in horizontal scale. It can filter out large-scale variation of surface temperature associated with the altitude of the ice

sheet and albedo fluctuation by atmospheric light absorption, mainly by water vapor, due to changing altitude and solar zenith angle.

Finally, we can select signals associated with surface



a



b

Fig. 2. (a) C pattern in high-pass filtered albedo image in Ch1 (bottom) and R2/1 (top) with resolution of 1.1 km on 4 December 1988 (left) and 3 December 1980 (right). White lines in each image show the location of profiles in Figure 3. (b) Surface contour map (NIPR, 1988) of Figure 2(a). North is N; solar azimuths of left and right figures are S and S' respectively. A corresponds to 0 km in Figure 3.

topography on the ice sheet by comparing different images. We selected cloud-free images from 360 data by checking both their temporal variability (Seko and others, 1992) and higher reflectance in Ch3 (mid-infrared: 3.5–3.7 μm) compared with the snow surface (NIPR, 1992). Further, we compared images which were taken 8 years apart, and conformed that the patterns we describe hereafter are almost stationary, at least on the scale of several years.

APPEARANCES OF UNDULATING TOPOGRAPHY

We describe three distinct patterns, based on the area in which they occur, temporally classified as C (coast, S (slope) and P (plateau). The areas where these three patterns were typically seen are shown in Figure 1.

C pattern

Figure 2a shows the high-pass filtered image of Ch1 (lower) and R2/1 (upper) on a coastal area of the ice sheet. Images taken under different solar azimuth are also shown to left and right.

The existence of distinct wavy structures in Ch1 is confined near the coast below 2000 m a.s.l., especially near the terminus of the outlet glacier (Shirase Glacier in Fig. 2b). The fluctuation of R2/1 develops not only below 2000 m a.s.l. but also higher. The C pattern has a wavelength of less than 10 km and is oriented normal to the ice flow lines deduced from surface contours (Fig. 2b).

Figure 3 shows profiles of the fluctuation in Ch1 and R2/1 along a flowline (white lines in Fig. 2a) of Shirase Glacier. Fluctuation in Ch1 is approximately $\pm 3\%$ and

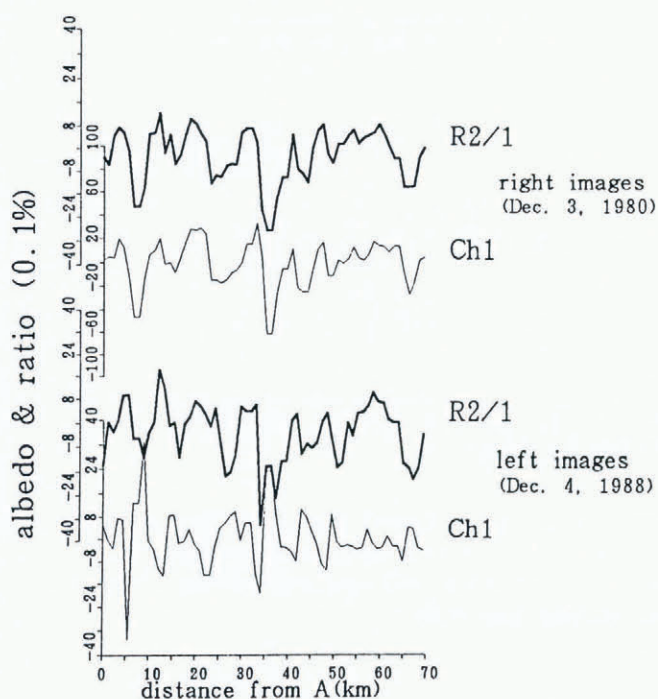
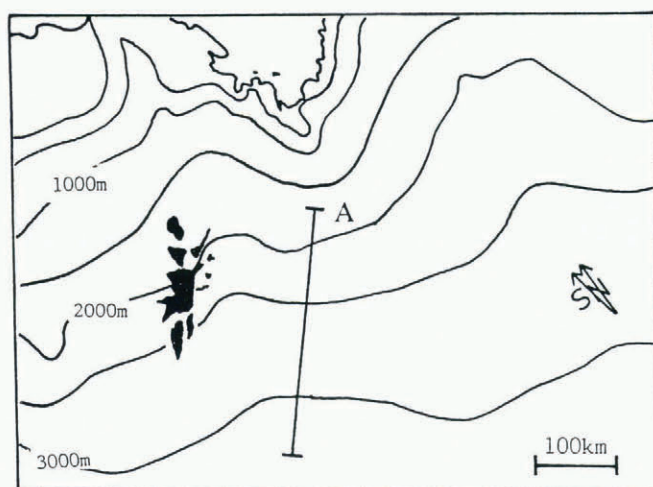


Fig. 3. High-pass filtered variations in Ch1 (thin lines) and R2/1 (thick lines) in C pattern on 4 December 1988 and 3 December 1980. Unit is 0.1%. The location of these profiles is shown in Figure 2(a) and (b).



a



b

Fig. 4:(a) High-pass filtered image of S pattern in R2/1 with a resolution of 2.2 km on 4 December 1988. (b) Surface contour map of the area (NIPR, 1988). The S and N are solar azimuth and north respectively. The central line shows the traverse route corresponding to profiles in Figure 5. A is 0 km in Figure 5(a), (b) and (c).

that in R2/1 is about $\pm 1.5\%$ in right images; in left images, they are both about $\pm 1.5\%$ except at a few points. The fluctuation in Ch1 and R2/1 is negatively and positively correlated in left and right image respectively, due to the solar azimuth (see below).

S pattern

A well defined fluctuation in spectral ratio (R2/1) develops from 2000 m to 3000 m a.s.l. (Fig. 4a). The wavelength is 10 km and 20 km at 2000 m and 3000 m a.s.l. respectively, gradually increasing with increasing altitude. The dominant alignment of stripes is at a right angle to the ice-flow lines (Fig. 4b) in the lower region around 2000 m a.s.l. or katabatic wind direction in the upper region (Seko and others, 1992).

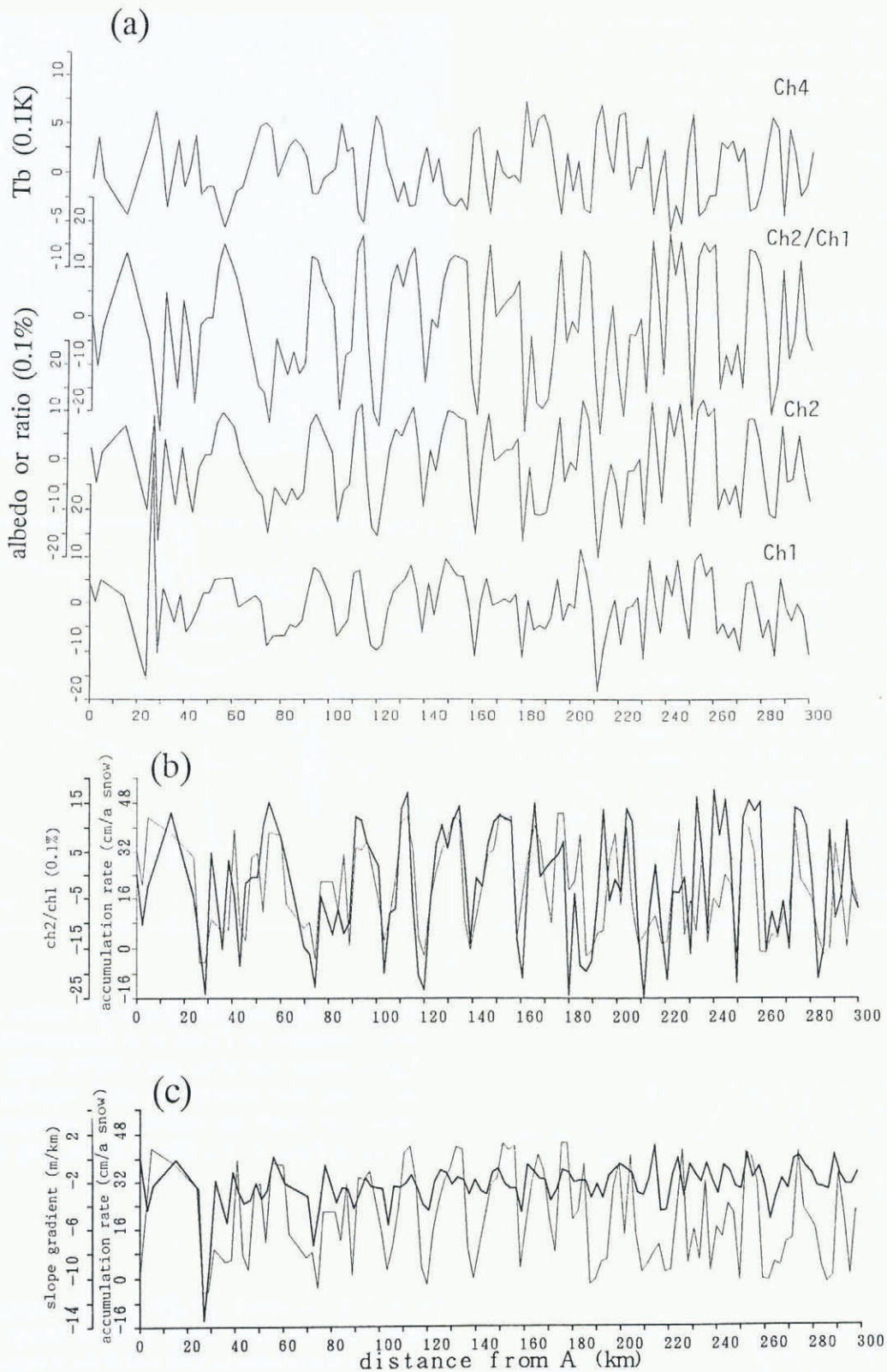


Fig. 5. (a) High-pass filtered profiles in channels 1, 2, 4 and R2/1 along the line in Figure 4b. Units are 0.1% in albedo or R2/1, and 0.1 K in Tb. (b) The relationship between accumulation rate (thin line) and high-pass filtered R2/1 (thick line) along the line shown in Figure 4b. (c) Relationship between accumulation rate (thin) and slope gradient (thick) along the line shown in Figure 4b. Large negative values in the slope mean steep slopes.

Fluctuation is not found only in R2/1 but also in Ch1, Ch2 and Ch4. Figure 5a shows profiles of these variations along an oversnow traverse line (a line in Fig. 4b). Fluctuations in Ch1, Ch2 and R2/1 are positively

correlated with each other and inversely correlated with the fluctuation in Ch4. The difference between S and C patterns is seen in the larger fluctuation in R2/1 (about $\pm 2\%$) than in Ch1 (about $\pm 1\%$) except at a few points

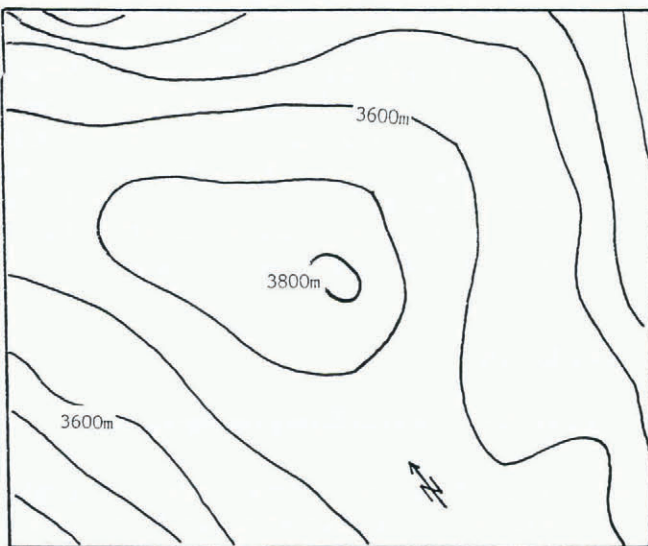
such as 25 km from "A". Fluctuations in Ch1 and R2/1 are positively correlated under different solar azimuth (not shown).

Figure 5b shows the relationship between R2/1 and the accumulation rate determined by measuring exposed snow-stake heights along an oversnow traverse route within four years from 1982 to 1986 (Nishio and others, 1988). Accumulation rate ranges from 0 cm a^{-1} to 40 cm a^{-1} snow, and there is fairly good agreement between them; low ratio corresponds to low accumulation rate.

Figure 5c shows the relationship between the net accumulation rate and the gradient of surface elevation measured by satellite Doppler positioning system and barometers (Nishio and others, 1988, a, b). It is also noticeable that low accumulation occurs on the steep slopes of the undulating topography. The amplitude of



a



b

Fig. 6. (a) P pattern in Ch4 image on 1 July 1988 with a resolution of 1.1 km. The white line and letter A in the center of the figure show the traverse route corresponding to profiles and 0 km in Figure 7 respectively. (b) Surface contour map (NIPR, 1988) of above.

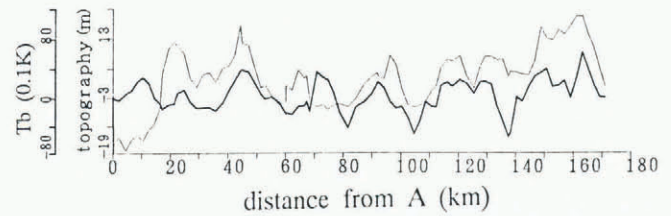


Fig. 7. High-pass filtered variations on surface topography (thin line) and the Tb (thick lines) along the over-snow traverse route in Figure 6(a).

the undulation along this line is about a few tens of meters and slope gradient ranges from -6×10^{-3} to -1×10^{-3} except at the steepest point 27 km from "A" in Figure 4b.

P pattern

P pattern can be seen on the ice-sheet surface on the further interior plateau above 3000 m a.s.l. It is clearly seen in winter Ch4 images, less so in summer Ch1 images and variation in R2/1 is negligible. Figure 6 shows an image on Ch4 focusing on the interior plateau of the ice sheet with a spatial resolution of 1.1 km. A band-shaped structure surrounds a summit of the ice sheet, with more than 20 km in horizontal spacing. Part of the band aligns at a right angle to ice flow lines deduced from surface contours, and part of the band is normal to katabatic wind directions which are partly seen as streak features in Ch4 (Seko, 1992; NIPR, 1992).

Figure 7 shows relationships between the fluctuations in Ch4 and the undulating topography measured by satellite Doppler positioning system and barometers during an over-snow traverse (Ageta and others, 1987). High Tb (brightness temperature) corresponds to the crest of undulating topography. The amplitude of the undulating topography along this line is deduced from the field data to be 8 m and slope gradient ranges from -2×10^{-3} to 1×10^{-3} ; the corresponding amplitude of fluctuation in Ch4 is about 4 K. Though the fluctuation in Ch1 in summer images is much smaller than that in C and S patterns, the wavelength of the fluctuation in Ch1 is similar to that in Ch4 and the surface topography.

THE CAUSE OF VISUALIZATION

We suggest plausible reasons for the visualization of undulating topography and surface properties on the undulating topography in several channels. We can deduce their characteristics from the multi-spectral data of AVHRR.

Visualization in reflectance and the spectrum

Undulating topography causes the change of solar irradiance per unit area and reflected energy is proportional to the irradiance. 1% of change in slope causes 1.7% of irradiance on unit area under 60° of the solar zenith angle. We can estimate the amplitude of undulating topography by checking the fluctuation of

reflected energy in Ch1 or Ch2 unless albedo varies greatly over the undulating topography.

Actual ice sheets, however, are composed of many types of surface (Watanabe, 1978) associated with different albedos. A spectral index ($R2/1$) is very useful to detect the fluctuation of surface properties because the effect of undulating slope can be eliminated by taking the ratio. Reflectance in the near-infrared channel (Ch2) is more sensitive to the change of snow grain-size than that in the visible channel (Ch1) (Wiscombe and Warren, 1980). Hence $R2/1$ should be the index which is proportional to the albedo on a snow surface. Reducing albedo by stronger sintering of snow particles probably occurs in lower-accumulation environment. Especially where net accumulation is almost zero, surface glazing is expected to occur. Fujii and others (1987) found that glazed surface can be detected as relatively low-albedo (low $R2/1$) areas in NOAA AVHRR.

If undulating topography and change of surface properties co-exist (and considered to occur commonly on the ice sheet), it is difficult to estimate each contribution to the fluctuation in a single channel. We can deduce the relative contribution of each effect by examining both fluctuations in Ch1 and $R2/1$. As we have seen in Figure 3, C pattern varies more in Ch1 than in $R2/1$, and in the image under a different solar azimuth, the fluctuation in Ch1 appears in an opposite sense but that in $R2/1$ remains in a similar sense. They also suggest the widely fluctuating slope in C pattern. In S pattern, contrastingly, the amplitude of fluctuation in $R2/1$ is larger than in Ch1 (Fig. 5a), showing that S pattern has less variation of slope than that in C pattern, but a large variation of accumulation, which is confirmed by ground-survey data (Fig. 5b).

On the steep slopes of undulating topography, it can be deduced that katabatic wind is accelerated and it results in low accumulation rate because of the divergence of blowing snow flux. It can be said that this relationship is generally seen in both C and S patterns from the phase relationship between the fluctuation in Ch1 and $R2/1$.

Visualization in thermal infrared channel

The inverse correlation between fluctuations in Ch1 and Ch2, and that in Ch4 in S pattern (Fig. 5a) is probably caused by the heat budget on the snow surface. In summer when little wind and relatively stronger sunshine exist, snow surface temperature is primarily affected by short-wave radiation budget. Hence, the fluctuation of albedo and/or slope inclination determines that of surface temperature.

P pattern was clearly detected in winter Ch4 images. In winter, a surface temperature inversion exists over the ice sheet, exceeding 20 K at the lowest 100 m on the inland plateau (Schwerdtfeger, 1984). If surface undulating topography exists, part of the radiative cooled air will drain into the depression between the crests. Ground-survey data (Fig. 7) show that the amplitude of the undulating topography (2×10^{-3}) exceeds the averaged slope gradient on the inland plateau of the ice sheet (1.5×10^{-3}). It can be considered that a part of surface air flow on the inland plateau is controlled by the undulation and we can detect the pools of cold air in the Tb fluctuations in Ch4.

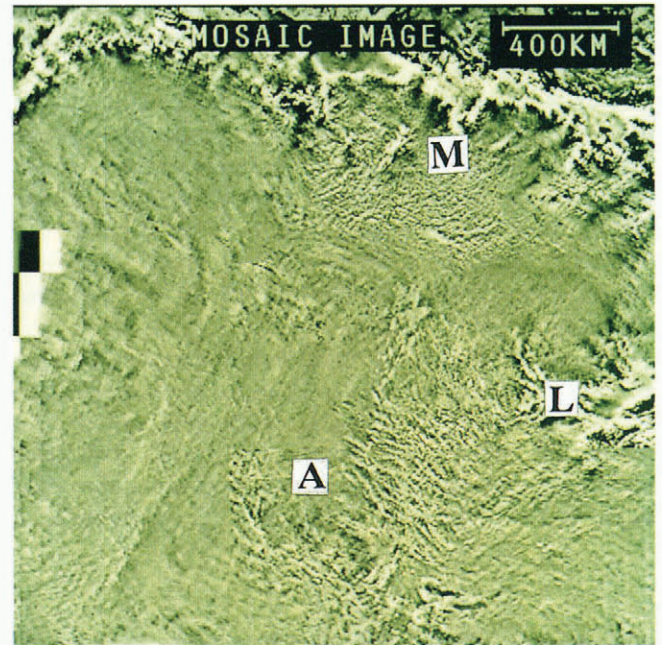


Fig. 8. Mosaic of Ch4 images with a resolution of 4.4 km constructed from 10 images in December 1988. L, M and A are Lambert Glacier, Mizuho Plateau and Dome A respectively.

AREAL DISTRIBUTION OF UNDULATIONS IN OTHER REGIONS

Fluctuations of albedo and Tb can be seen in several regions on the ice sheet. To illustrate the occurrence of the fluctuation over a wide area, a mosaic of 10 cloud-free images with a resolution of 4.4 km was constructed (Fig. 8).

While the resolution is poor, the distribution of fluctuation in Ch4 can be seen in this image as band-shaped structures. Fluctuations probably correspond to C or S pattern according to the classification in the previous section. Remarkable fluctuations can be seen in the drainage basin area of Lambert Glacier (L) and Mizuho Plateau (M). No apparent fluctuation is found in ridges and the interior plateau on the ice sheet except southwestern flank of Dome A (A). It is interesting that the fluctuation does not develop all over below 3000 m a.s.l. and it can be found on the valley-shaped area in horizontal scale of 1000 km such as M or L.

DISCUSSION

Characteristics of undulating topography

It is reasonable to say that, while undulating topography can be found at every altitude on the ice sheet, causes of visualization in AVHRR differed. We classified them into three patterns. Characteristics of each pattern of undulating topography are summarized in Table 1.

Alignment and wavelength are readily observed from the images, and provide useful information of ice-sheet dynamics. The change of wavelength with altitude is similar to the ground-survey data compiled by McIntyre

Table 1. Characteristics of each pattern

Region	C (Coast)	S (Slope)	P (Plateau)
altitude (m)	0–2000	2000–3000	3000–4000
mean slope	1×10^{-2}	6×10^{-3}	1.5×10^{-3}
wavelength (km)	5–10	10–20	20–25
orientation (normal to wind)	ice flow	katabatic wind ice flow	ice flow katabatic
anomaly of accumulation	large (estimated)	large (40 cm a^{-1})	small (estimated)
amplitude of undulating topography	1.5×10^{-2}	4×10^{-3}	2×10^{-3}
amplitude of fluctuation in Ch1 (%)	2.5	1.5	0.5
amplitude of fluctuation in R2/1 (%)	1.5	2	negligible

(1986) and the wave length of P pattern is similar to that Zwally and others (1983) found from the satellite microwave altimetry near Dome A.

Although knowing their vertical scale is useful for understanding ice dynamics, it is difficult to calculate the amplitude of undulations from AVHRR, since reflectance is affected not only by undulating slope but also by albedo and/or subgrid-scale topographies such as sastrugi (Wendler and Kelley, 1988). Actually, the surface properties change as seen in the fluctuation R2/1 in C and S patterns. The amplitude of P pattern cannot be estimated by fluctuations in Ch4, because the surface temperature inversion strength can vary under daily meteorological conditions. Hence, we show here the amplitudes of the undulating topography along over-snow traverse lines in S and P patterns. Concerning C pattern in which we have no ground-survey data, the amplitude was estimated as an averaged value of the fluctuation in Ch1 in two different images under almost opposite solar azimuth (Fig. 3), because, at least, the actual amplitude of the undulating topography must lie between these values.

Origins of undulating topography

A simple theoretical study (Nye, 1959) shows that the life span of the surface undulating topography is less than 10 years, assuming 3000 m thickness of ice, 10 m a^{-1} of ice-

flow speed and no supporting force. Hence, undulating topography existing on the ice sheet must be supported by some forces. One possibility is subglacial topography, another could be accumulation anomalies.

The appearance of C pattern reflects the effect from subglacial topography. Its absence on ice shelf (NIPR, 1992) may show that it is the result of subglacial effect. On the edge of an ice sheet where ice is thinner and moves faster than inland, the effect of subglacial topography on the surface topography is greater. Some correspondence between undulating surface topography and subglacial topography was reported along a line shown in Figure 5c (Nishio and others, 1988a).

The relationship between accumulation and surface slope gradient (Fig. 5c) suggests a prevailing wind process. Anomalously accumulated snow changes topography, and katabatic wind can be affected by surface topography of a few tens of km in horizontal scale (Kikuchi and Ageta, 1989). Considering the variation of accumulation is 40 cm a^{-1} (Fig. 5b) and the surface topography has an amplitude 10 m, the wind action can alter a topography within 100 years. It could be a candidate to modify the topography primarily formed by bedrock undulation, and the alignment of undulation normal to the katabatic wind may suggest that wind processes modify this topography.

CONCLUSION

Undulating topography on the Antarctic ice sheet was revealed by fluctuation of albedo, the ratio of albedos and thermal infrared channel of NOAA AVHRR. The advantage of AVHRR is its wide areal coverage which encompasses from the coast to the inland plateau of the ice sheet.

By applying a spatial high-pass filter, we can enhance the information associated with undulating topography. The variation of reflectance in Ch1 and the change of the variation under different solar azimuth provides information of amplitude of topography. R2/1 has information on surface properties especially affected by accumulation anomaly.

While the quantitative interpretation of characteristics of the undulating topography from AVHRR alone is limited, the characteristics of the undulating topography in each region on the ice sheet (Table 1) contain information about dynamics and climatological conditions on the ice sheet. As a result, the following characteristics of undulating topography were detected.

- (1) The wavelength of undulating topography is narrower and the amplitude is larger in a coastal area; spacing becomes wider and amplitude smaller in an inland region.
- (2) Accumulation anomaly associated with the undulating topography can be detected by fluctuations of R2/1. Large fluctuations can be seen below 3000 m a.s.l.
- (3) Below 3000 m a.s.l., a steep slope in the undulating topography generally corresponds to a low accumulation area.

- (4) The development of undulating topography and/or an associated accumulation anomaly below 3000 m a.s.l. is confined to a few regions, for example near the terminus of an outlet glacier or a valley-shaped drainage area.

By using AVHRR together with ground-survey data and/or satellite altimetry, more comprehensive analyses of the surface condition on the ice sheets becomes available, and it can also be utilized for selecting good coring sites for climate study.

ACKNOWLEDGEMENTS

The authors greatly thank Dr T. Yamanouchi, National Institute of Polar Research, for useful advice in this study. Some fine resolution data were processed by Mr H. Sakurai, NIPR. FIVIS image-processing system of the Nagoya University computation center was used for image processing.

REFERENCES

- Ageta, Y., T. Kikuchi, K. Kamiyama and F. Okuhira. 1987. Glaciological research program in east Queen Maud Land, East Antarctica. Part 5. 1985. *JARE Data Rep.* 125.
- Bindschadler, R. A. and P. L. Vornberger. 1990. AVHRR imagery reveals Antarctic ice dynamics. *EOS*, **71**(23), 741–742.
- Budd, W. F., R. J. Dingle and U. Radok. 1966. The Byrd Snow Drift Project: outline and basic results. *Antarct. Res. Ser.*, **9**, 71–134.
- Fujii, Y., T. Yamanouchi, K. Suzuki and S. Tanaka. 1987. Comparison of the surface conditions of the inland ice sheet, Dronning Maud Land, Antarctica, derived from NOAA AVHRR data with ground observation. *Ann. Glaciol.*, **9**, 72–75.
- Furukawa, T., O. Watanabe, K. Seko and Y. Fujii. 1992. Distribution of surface conditions of ice sheet in Enderby Land and east Queen Maud Land, East Antarctica. *Proceedings of the NIPR Symposium on Polar Meteorology and Glaciology* 5, 140–144.
- Kikuchi, T. and Y. Ageta. 1989. A preliminary estimate of inertia effects in a bulk model of katabatic wind. *Proceedings of the NIPR Symposium on Polar Meteorology and Glaciology* 2, 61–69.
- McIntyre, N. F. 1986. Antarctic ice-sheet topography and surface–bedrock relationships. *Ann. Glaciol.*, **8**, 124–128.
- National Institute of Polar Research (NIPR). 1988. *East Queen Maud Land–Enderby Land*. Tokyo, National Institute of Polar Research.
- Nishio, F., H. Ohmae and M. Ishikawa. 1988a. Bedrock and ice surface profiles in the Shirase Glacier basin determined by the ground-based radio-echo sounding. *Bull. Glacier Res.* **6**, 33–39.
- Nishio, F., H. Ohmae and K. Osada. 1988b. Glaciological research program in east Queen Maud Land, East Antarctica. Part 7. 1986. *JARE Data Rep.* 137.
- Nye, J. F. 1959. The motion of ice sheets and glaciers. *J. Glaciol.*, **3**(26), 493–507.
- Orheim, O. and B. K. Lucchitta. 1987. Snow and ice studies by Thematic Mapper and multispectral scanner Landsat images. *Ann. Glaciol.*, **9**, 109–118.
- Orheim, O. and B. K. Lucchitta. 1988. Numerical analysis of Landsat Thematic Mapper images of Antarctica: surface temperatures and physical properties. *Ann. Glaciol.*, **11**, 109–120.
- Schwerdtfeger, W. 1984. *Weather and climate of the Antarctic*. Amsterdam, Elsevier.
- Seko, K. 1992. Preliminary study of katabatic wind by using NOAA AVHRR data. *Proceedings of the NIPR Symposium on Polar Meteorology and Glaciology* 5, 167–173.
- Seko, K., T. Furukawa and O. Watanabe. 1992. Surface condition on the Antarctic ice sheet. In *Proceedings of the Conference on the Role of the Polar Region in Global Climate, Alaska University, Fairbanks*, 238–242.
- Stephenson, S. N. and R. A. Bindschadler. 1990. Is ice-stream evolution revealed by satellite imagery? *Ann. Glaciol.*, **14**, 273–277.
- Swithinbank, C. 1988. Satellite image atlas of glaciers of the world. Antarctica. *U.S. Geol. Surv. Prof. Pap.* 1386-B.
- Watanabe, O. 1978. Distribution of surface features of snow cover in Mizuho Plateau. *Mem. Natl. Inst. Polar Res. Spec. Issue* 7, 44–62.
- Wendler, G. and J. Kelley. 1988. On the albedo of snow in Antarctica: a contribution to I.A.G.O. *J. Glaciol.*, **34**(116), 19–25.
- Wiscombe, W. J. and S. G. Warren. 1980. A model for the spectral albedo of snow. I. Pure snow. *J. Atmos. Sci.*, **37**(12), 2712–2733.
- Yamanouchi, T. and K. Seko, *comps.* 1992. *Antarctica from NOAA satellites — clouds, ice and snow*. Tokyo, National Institute of Polar Research.
- Zwally, H. J., R. A. Bindschadler, A. C. Brenner, T. V. Martin and R. H. Thomas. 1983. Surface elevation contours of Greenland and Antarctic ice sheets. *J. Geophys. Res.*, **88**(C3), 1589–1596.

The accuracy of references in the text and in this list is the responsibility of the authors, to whom queries should be addressed.